Journal of Materials Chemistry A

Accepted Manuscript

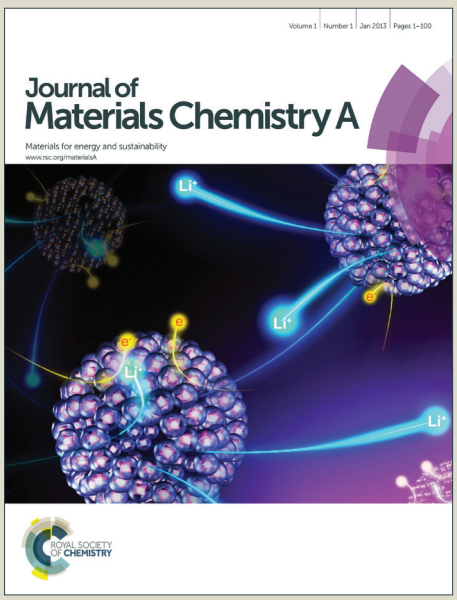

ROYAL SOCIETY OF CHEMISTRY

www.rsc.org/materialsA

Materials Chemistry A

ARTICLE

Co_3O_4/Porous Electrospun Carbon Nanofibers as Anodes for High Performance Li-ion Batteries

Cite this: DOI: 10.1039/x0xx00000x

Received 00th June 2014,
Accepted 00th June 2014

DOI: 10.1039/x0xx00000x

www.rsc.org/

Sara Abouali,[a] Mohammad Akbari Garakani,[a] Biao Zhang,[a] Hui Luo,[a] Zheng-Long Xu,[a] Jian-Qiu Huang,[a] Jiaqiang Huang[a] and Jang-Kyo Kim[a]*

This paper reports a facile route to synthesize porous carbon nanofibers containing cobalt and cobalt oxide nanoparticles (CoO_x/PCNF) as anodes for Li-ion batteries. The Co_3O_4/PCNF electrode delivers a remarkable capacity of 952 mAh g^{-1} after 100 cycles and equally excellent rate performance at high current densities. There are several ameliorating mechanisms responsible for the observation: namely (i) high theoretical capacity of Co_3O_4 particles; (ii) enhanced electronic conductivity and Li ion transfer due to the graphene layers surrounding the Co_3O_4 particles; (iii) the soft CNF matrix serving as the stress buffer to relieve the volumetric stresses arising from Li ion insertion into the Co_3O_4 particles. The comparison of electrochemical performance with previous studies based on similar CoO or Co_3O_4/carbon composite anodes indicates the above value is among the highest.

Introduction

Rechargeable Li-ion batteries (LIBs) have attracted much attention as an important energy storage device due to their high energy density and design flexibility which finds many applications in a wide variety of devices, such as cell phones, laptops and electric vehicles.[1-3] One of the most critical components that affect the performance of LIBs is the anode material. Commercial LIBs use graphite as the anode material which has a low theoretical capacity of 372 $mAhg^{-1}$.[4] Hence, there has been extensive research to replace the graphite with a high capacity material. Transition metal oxides have been introduced with varied successes which possess much higher theoretical capacities than carbonaceous materials.[5] Among these, mixed-valent cobalt oxide, Co_3O_4, with an inverse spinel structure has been considered an attractive choice due to its high theoretical capacity of 890 $mAhg^{-1}$– more than twice that of graphite – which can meet the demanding application in electric vehicles.[6] The Li storage mechanism of Co_3O_4 was investigated,[7] showing the reversible conversion reaction which resulted in storing 8 mole of Li per mole of Co_3O_4. Since then, a few different structures of Co_3O_4 have been investigated, including nanosheet-assembled multi-shelled hollow spheres, [8] nanotubes, nanorods and nanoparticles.[9] The comprehensive recent review[10] provides useful information on various types of metal oxides and their relative advantages and weaknesses as anodes for LIBs. However, the relatively large initial irreversible capacity and poor cyclic stability originating from the large volumetric expansion/contraction and severe particle aggregation during the Li ion insertion/extraction processes have limited the application of Co_3O_4 in practical LIBs. Besides, similar to other metal oxides, it suffers from a poor electrical conductivity, leading to capacity degradation upon charge/discharge cycles.[10]

A few different strategies have been proposed to overcome the aforementioned issues. One of the most promising methods is to uniformly disperse nanostructured metal oxides in a carbonaceous matrix which can simultaneously benefit from the high electrical conductivity and cyclic stability of carbon.[11, 12] Different carbon allotropes have been employed as the support

or matrix for the high-capacity active nanoparticles, such as activated carbon, carbon coatings, carbon nanotubes (CNTs) and graphene.[13-15] For example, nanocomposites containing Co_3O_4/graphene,[6,13] Co_3O_4/CNT[14] and Co_3O_4/carbon spheres[15] have been successfully synthesized which showed improvements in specific capacity and rate capability. Although their morphologies were different, these carbon materials functioned two common tasks: namely (i) to serve as stress buffer to release the volumetric stresses through the soft matrix; and (ii) to serve as conductive paths for fast Li ion and electron transfer. However, further enhancements are necessary to prevent fast capacity fading of the electrodes. Furthermore, the reported synthesis methods included multi-step processes and usually employed hazardous chemicals, which make the preparation complicated and limit large-scale applications. Designing a facile one-step strategy to synthesize these high capacity electrodes has been the biggest challenge.

Electrospinning is a facile, low-cost technique to produce continuous carbon nanofibers (CNFs) in the form of thin films by applying a strong electric field between the nozzle and collector while injecting a polymer solution. The one-step process employs low-cost polymers as the carbon precursor, seldom involving hazardous chemicals; and it can be easily scaled up for mass production in commercial applications. The CNF films produced thereby are freestanding, and can be used directly as the electrodes without adding polymer binders or conductive additives, They possess many advantages over the other forms of carbon or processing methods, such as easy and controllable creation of extremely large surface area and hierarchical pores as well as tunable compositions of the CNF composites by *in situ* incorporating active materials and/or conductive additives. All these advantages resulted in attractive electrochemical properties of the electrodes made therefrom.[16-18]. Herein, we report a one-pot strategy to produce Co and Co_3O_4 nanoparticles embedded in electrospun porous carbon nanofibers (CoO_x/PCNF). Spherical Co_3O_4 nanoparticles were surrounded by graphitic carbon shells in the CNF matrix. The composite electrodes showed excellent cyclic and rate performance resulting from the high capacity spinel cobalt oxides and improved conducting networks provided by the graphitic carbon layers and CNFs . All these benefits make this hybrid material a good candidate as electrodes in high performance LIBs.

Experimental

Materials and Methods

Polyacrilonitrile (PAN, Average Mw=150k supplied by Aldrich) and polymethyl methacrylate (PMMA, Average Mw=15k supplied by Aldrich) were used as precursors and N, N-dimethylformamide (DMF) as the solvent to produce the porous carbon nanofibers (PCNF) matrix. Cobalt (II) acetate tetrahydrate (CoAc, supplied by UNI-CHEM) was used as the source of Co. 0.4 g PAN, 0.3 g PMMA and 0.3 g CoAc were dissolved in 10 ml of DMF at 80 ˚C for 5 h under magnetic stirring. The mixture was transferred to a plastic capillary and electrospun on a spinning machine (KATO Tech. Co., Japan) at 16 kV. The collector to needle distance was kept constant at 15 cm to collect a light-pink film on an aluminum foil wrapped around a drum collector rotating at a speed of 0.6 m min^{-1}. The film was stabilized at 250 ˚C for 90 min in air and carbonized at 650 ˚C for 1 h in a nitrogen atmosphere using a tube furnace. Both the temperatures and durations for stabilization and carbonization were chosen after extensive preliminary experiments. Although carbonization at temperatures higher than 650℃ was beneficial to improving the electrical conductivity of the carbon matrix, it resulted in coarsening of Co nanoparticles, detrimental to electrochemical properties of the electrodes. A lower temperature or a shorter duration, however, was only caused incomplete crystallization of the nanoparticles. The resultant CNFs consisted of Co nanoparticles uniformly dispersed in the porous carbon matrix, which is designated as Co/PCNF. The carbonized films were post-heat treated at 300 ˚C for 15 min in air to precipitate Co_3O_4 nanoparticles, designating the final product as Co_3O_4/PCNF. Two important factors were taken into consideration in selecting the optimized oxidation condition: namely, (i) a temperature sufficiently high to oxidize the Co nanoparticles to produce a Co_3O_4 phase, and (ii) a low temperature to prevent burning of carbon in an oxygen atmosphere. Having tried many different oxidation temperatures and times, the above combination was finally chosen. For comparison, neat non-porous carbon nanofibers (CNFs) and neat porous carbon nanofibers (PCNFs) were also produced without the CoAc precursor using the same procedure. The schematic of the synthesis process is shown in Fig.1.

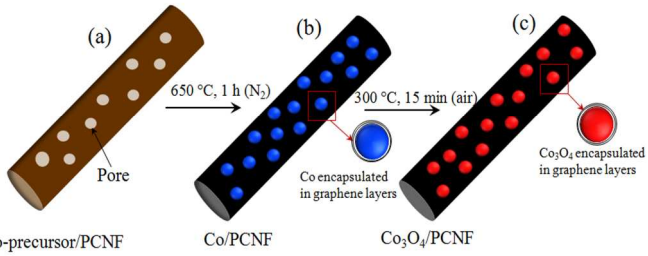

Fig. 1 Schematic illustration of the synthetic process (a) Co-precursor/PCNF after stabilization; (b) Co/PCNF after carbonization and (c) Co_3O_4/PCNF after post-heat treatment.

Structural Characterization

The microstructures and morphologies of the materials were studied on a scanning electron microscope (SEM, JEOL 6300) and a field emission transmission electron microscope (FETEM, JEOL 2010F). The crystal structure was studied on a powder X-ray diffraction (XRD) system (PW1830, Philips) with Cu Kα radiation. The X–ray photoelectron spectroscopy (XPS, Surface analysis PHI5600, Physical Electronics) was employed to evaluate the surface chemistry of the materials, using a monochromatic Al Kα X-ray at 14 kV. Thermogravimetric analysis (TGA) was conducted (TGA/DTA 92 Setaram II testing system) in air over a temperature range of 50–800 ˚C at a heating rate of 10 ˚C min^{-1}.The electrical conductivities were also measured using a four-probe method.

Electrochemical Measurements

Electrochemical tests were carried out using CR2032 coin cells. The PCNF and Co/PCNF electrodes were prepared without adding binder as the freestanding films. The Co_3O_4/PCNF electrode was prepared by mixing the active material with conductive carbon black (super P) and polyvinylidene fluoride (PVDF) as the binder dissolved in N-methyl-2-pyrrolidone (NMP) in the weight ratio of 80:10:10. The slurry was coated onto a copper foil, from which pellets of 12mm in diameter were cut to use as electrodes. The cells were assembled in an Ar-filled glove box with a Li foil as counter electrode, $LiPF_6$ (1

M) in ethyl carbonate (EC)/dimethyl carbonate (DMC) (1:1 by volume) as electrolyte and a microporous polyethylene film (Celgard 2400) as separator. The coin cells were subjected to cyclic tests between 0 and 3 V at different current densities on a battery tester (LAND 2001 CT). The cyclic voltammetry (CV) tests were performed between 0 and 3 V at a scan rate of 0.1 mV s^{-1} on an electrochemical workstation (CHI660c). The mass loading of the active material (= 1 mg), including both Co_3O_4 and PCNF, were taken into account when the capacities were calculated.

Results and Discussion

The SEM and TEM images of both CNFs and PCNFs after carbonization at 650 °C are given in Fig. 2, showing bead-free nanofibers with uniform diameters ranging between 100 and 300 nm (insets in Figs. 2a and 2b). From the contrast difference between them, it is obvious that the neat CNFs were non-porous and completely solid (Fig. 2a), whereas the PCNFs contained a large number of pores with elongated shapes (Fig. 2b). These pores have been formed as a result of decomposition of PMMA during heat treatment. The BET surface area of the PCNF sample was measured to be ~33 $m^2 g^{-1}$ and the majority of the pores were less than 10 nm in diameter (Fig. S1 and Table S1). By comparing the surface area of the non-porous CNFs reported in our previous work (14 $m^2 g^{-1}$) for the same material,[19] the surface area of PCNFs has been approximately doubled by adding PMMA as the sacrificial polymer. The morphologies of the as-spun nanofibers containing CoAc precursor (Figs. 3a, 3b) were much the same as those without. In order to better understand the formation of pores and Co_3O_4 nanoparticles, the nanofibers were examined under TEM after each heat-treatment step.

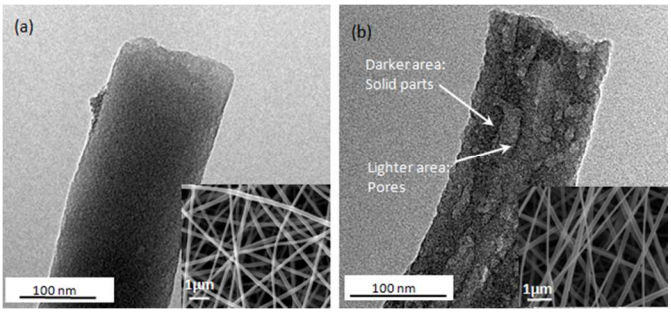

Fig. 2 (a) TEM and SEM (inset) images of neat non-porous carbon nanofibers (CNFs); and (b) TEM and SEM (inset) images of porous carbon nanofibers (PCNFs) after carbonization at 650 °C for 1 h.

During electrospinning, the CoAc precursor was dispersed in the nanofibers, and upon stabilization at 250 ˚C, cobalt acetate lost water according to the reaction (1):

$$Co(CH_3COO)_2.4H_2O \rightarrow Co(OH)(CH_3COO)+3H_2O+CH_3COOH \quad (1)$$

Meanwhile, the volatile and non-carbon elements in PAN matrix started disappearing while PMMA was partially decomposed to form pores in the nanofibers. Although no obvious Co nanoparticles were detected from the TEM image (Fig. 3b), the elemental maps given in Figs. S2a-c clearly identified the dispersion states of C, Co and O elements. Once carbonized at 650 ˚C, the PMMA phase was decomposed completely and the PAN matrix was transformed into amorphous carbon. At this stage, cobalt acetate was decomposed to cobalt monoxide (CoO) according to the reactions (2) and (3). Due to the high temperature process in an inert atmosphere, CoO was reduced to metallic Co according to the reaction (4).[20]

$$Co\,(CH_3COO) \rightarrow 0.5CoO + 0.5CoCO_3 + 0.5H_2O + 0.5CH_3COCH_3 \quad (2)$$

$$CoCO_3 \rightarrow CoO + CO_2 \quad (3)$$

$$CoO + CO \rightarrow Co + CO_2 \quad (4)$$

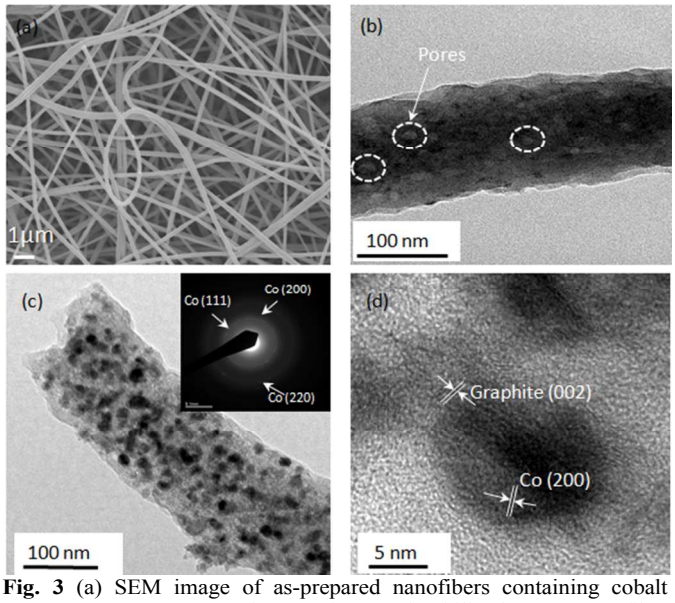

Fig. 3 (a) SEM image of as-prepared nanofibers containing cobalt acetate, CoAc, precursor; (b) TEM image of stabilized porous nanofiber, CoAc/PCNFs; (c) TEM and SAED pattern of carbonized nanofiber, Co/PCNF, and (d) HRTEM of nanoparticles in (c).

The nanofiber obtained after carbonization, Co/PCNFs, contained numerous crystalline nanoparticles of diameters ranging from 15 to 30nm, as shown in Fig. 3c. The selected area electron diffraction (SAED) pattern given in the inset, confirmed that they were metallic Co which is in agreement with Equation (4). The HRTEM image in Fig. 3d indicates that the Co nanoparticles were surrounded by a few graphene layers with d-spacing of 0.34 nm, which were created due to the catalytic effect of metallic Co on graphitization.[19] The graphene layers could not only firmly hold the nanoparticles, but also improve the electrical conduction of the local amorphous carbon matrix.

To produce Co_3O_4 nanoparticles, a carefully chosen post-heat treatment in air was necessary to oxidize the metallic Co into Co_3O_4 without decomposition of CNFs. Longer durations or higher temperatures often led to complete burning of carbon, while shorter durations or lower temperatures were not sufficient to oxidize Co to Co_3O_4. Because the Co nanoparticles were very fine and the fibers were highly porous, oxygen could easily react with Co particles although some were encapsulated within the CNFs. The morphologies and structure of the material thereby obtained, Co_3O_4/PCNF, are shown in Fig. 4, indicating the particle size ranged from 5 to 20 nm (Figs. 4a and 4b). The ultrafine crystalline Co_3O_4 nanoparticles were encapsulated by graphene layers that appeared to have grown further by adding more layers to a thickness about 2-4 nm during the post-heat treatment. This observation also indicates the stability of CNFs synthesized in this study. The XRD pattern (Fig. 4c) shows prominent peaks at 2Θ = 31.2, 36.8, 44.8, 55.6, 59.3 and 65.2˚ corresponding to the (220), (311),

(400), (422), (511) and (440) reflections of Co_3O_4 (JCPDS no. 078-1970). The SAED pattern (Fig. 4d) also confirmed Co_3O_4 nanoparticles. The above XRD and HRTEM results partly confirmed that the heat treatment conditions were well optimized to produce pure Co_3O_4 nanoparticles without burning carbon.

The results from the XPS analysis are shown in Figs. 5 and S3, and the atomic concentrations of major elements are summarized in Table 1. The deconvoluted C 1s spectra (Fig. 5a) showed four binding energies at 284.7, 286.2, 288.5 and 290.7 eV, corresponding to C-C, C-N, C=O and O=C-O functional groups, respectively.[19, 21] The Co 2p spectrum of Co/PCNF (Fig. 5b) exhibited a main peak at 778.4 eV for Co° and two plasmon losses appeared at 780 and 783.1 eV which are typical for conductive metals.[22, 23] For Co_3O_4/PCNF, two main peaks appeared at 779.8 and 781.4 eV corresponding to Co $2p_{3/2}$ and a satellite at 786.2 eV, in agreement with the previous reports for Co_3O_4.[24, 25] The O 1s spectra (Fig. 5c) showed three peaks at 531.3, 533.2 and 536.2 eV attributed respectively to the oxygen bonds in C=O, C-O and adsorbed surface water, while an extra peak appears at 529.8 eV for Co_3O_4/PCNF showing the oxygen species in cobalt spinel oxide.[25-27] The XPS elemental analysis indicates that the Co_3O_4/PCNF composite contained approximately 36 % of Co_3O_4, which is much lower than 67.7 wt.% obtained from the TGA curve (Fig. S4). The discrepancy arose mainly from the very shallow penetration depth of X-ray photoelectrons, i.e. only ~5 nm, while the Co_3O_4 particles were mostly embedded inside the CNFs. The TGA curve indicates that a weight loss started to occur at below 220 °C with a rapid weight loss in the temperature range of 330-430 °C due to burning of carbon, after which there was a steady weight.

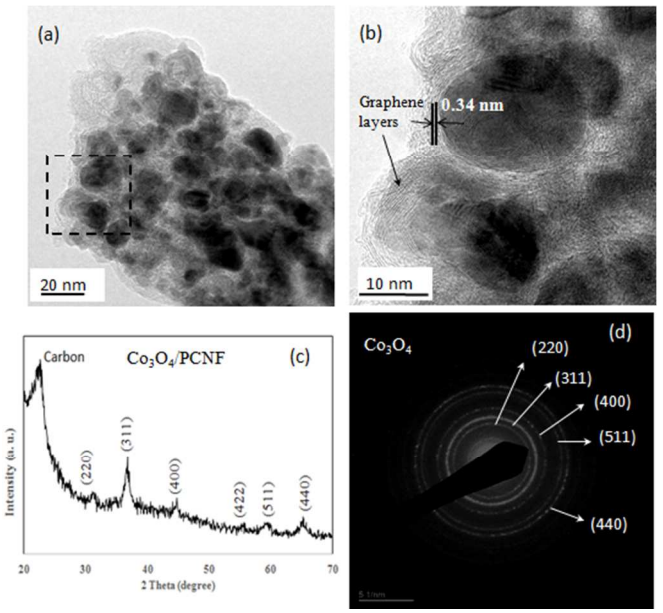

Fig. 4 Structure and characteristics of Co_3O_4/PCNF composite: (a) TEM image, (b) HRTEM image of nanoparticles, (c) XRD and (d) SAED patterns.

The electrochemical properties of the Co_3O_4/PCNF electrode measured in the voltage window of 0.01-3.0 V are compared with those of the neat PCNF and Co/PCNF electrodes in Fig. 6. The discharge/charge profiles of the Co_3O_4/PCNF electrode (Fig. 6a) presented a long plateau at about 1.03 V, followed by a slope down to 0.01V upon the first discharge. The crystalline Co_3O_4 phase was transformed to an amorphous state during the conversion reaction so that the voltage plateau gradually disappeared upon further cycles.[28] The CV curves of the Co_3O_4/PCNF electrode are shown in Fig. 6b. In the first cycle, a large cathodic peak appeared at 0.8 V corresponding to lithiation of Co_3O_4 to Co, followed by a small peak at around 0.36 V corresponding to the formation of a solid electrolyte interphase (SEI) film at below 0.8V. The main anodic peak observed at about 2.1 V is attributed to delithiation of Co to Co_3O_4. The very small anodic peak at 1.35 V suggests that oxidation took place in a multistep process. In the following cycles, the main cathodic peak splitted into two appearing at higher voltages. Upon reaching 0 V, another small cathodic peak emerged due to the insertion of Li ions into the CNF matrix. The significant difference in lithiation voltage is attributed to the changes in Co_3O_4 structure and SEI film, according to a recent study on the structural evolution of Co_3O_4 during cycles.[29] The overlapping of the CV curves of the subsequent 2^{nd}-5^{th} cycles confirmed excellent electrochemical reversibility of the electrode.

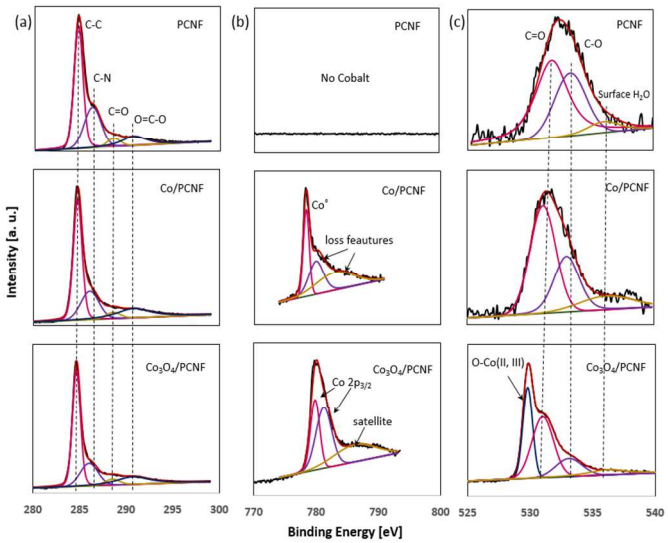

Fig. 5 Deconvoluted XPS spectra of (a) C 1s, (b) Co 2p and (c) O 1s.

The cyclic behaviors shown in Figs. 6c and S5 clearly indicate superior performance of the Co_3O_4/PCNF electrode. It is also interesting to note that the existence of Co nanoparticles in the PCNF matrix increased the capacity by ~ 33 % in comparison with the neat PCNF. This observation can be attributed to the enhanced electrical conductivity from 5.2×10^{-5} to 2.8 S/cm due to the presence of conducting Co particles (Table 1). In addition, the metallic nanoparticles also had an ameliorating catalytic effect on graphitization of the surrounding amorphous carbon which in turn led to a further increase in conductivity.[19] The first discharge and charge capacities of Co_3O_4/PCNF were 1187 and 1006 $mAhg^{-1}$, respectively, with a Coulombic efficiency of 84.7 %. These initial capacities are higher than the theoretical capacity 890 $mAhg^{-1}$ of neat Co_3O_4, due probably to the formation of a SEI film on the surface of the electrode. After 100 cycles, the discharge/charge capacities were reduced to 952/923 $mAhg^{-1}$ with a Coulombic efficiency of 97 %. These values are at least 250-450 $mAhg^{-1}$ higher than the corresponding values of the neat PCNF and Co/PCNF electrodes within the tested cycles. The homogeneous distribution of high capacity Co_3O_4 nanoparticles inside the porous CNFs, increased electron transport and electrical

conductivity through the 1D structure of CNFs as well as buffering of the mechanical stresses arising from the volumetric changes of Co_3O_4 particles upon cycles are the main reasons for this superior performance.[29-31] The onion-like graphene layers surrounding the Co_3O_4 nanoparticles also played an important role in improving the performance of the electrode after long cycles. Apart from enhanced electrical conductivities, they served as a sheath to avoid the detachment of the nanoparticles from the CNF matrix and thus to maintain the integrity of the hybrid material.[32, 33] The surge in capacity for the initial 15 cycles of the Co_3O_4/CNF electrode may be related to the gradual activation of the Co_3O_4 nanoparticles within the CNFs and the formation of SEI films.

Table 1. Atomic concentrations of the elements and electrical conductivities of PCNF, Co/PCNF and Co_3O_4/PCNF samples.

Samples	Compositions [at%]				Conductivity [S cm^{-1}]
	C	N	O	Co	
PCNF	86.7	10.4	2.88	-	5.2×10^{-5}
Co/PCNF	89.5	4.8	2.9	2.62	2.8
Co_3O_4/PCNF	75.59	1.2	16.07	7.14	4×10^{-3}

All electrode materials exhibited gradual decay of capacity with increasing current density (Fig. 6d). The Co_3O_4/PCNF electrode outperformed the Co/PCNF counterpart until the current density reached 1 A g^{-1}. This observation was expected because of the exceptional electrical conductivity of the latter which is three orders of magnitude higher than the former electrode (Table 1). However, the capacity was completely recovered when the current density was returned to 100 mAg^{-1}, indicating excellent electrochemical reversibility and structural integrity of the Co_3O_4/PCNF electrode.[28, 29]

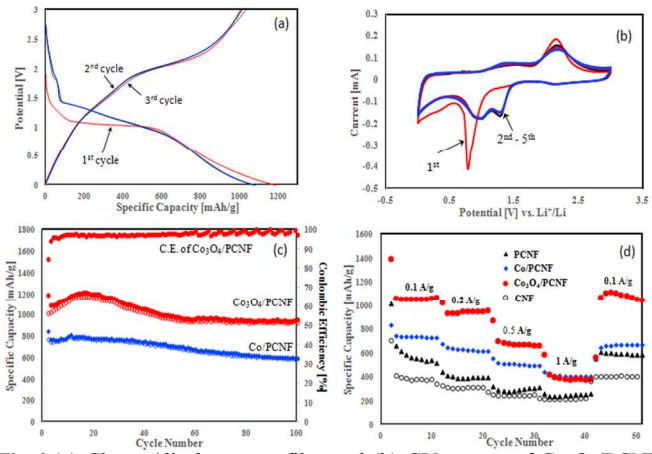

Fig.6 (a) Charge/discharge profiles and (b) CV curves of Co_3O_4/PCNF electrode; (c) cyclic performance at a current density of 0.1 Ag^{-1} and (d) rate performance of neat CNF, PCNF, Co/PCNF and Co_3O_4/PCNF electrodes.

The electrochemical performance is compared between the present electrode and those of previous similar works based on CoO or Co_3O_4 particles embedded in carbon substrates as shown in Table 2. The capacity of the Co_3O_4/PCNF electrode synthesized in the current study is among the highest, suggesting that the electrode material can be a good candidate as anode material in high performance LIBs.

Table 2. Comparison of specific capacities of Co_3O_4/PCNF electrode with similar CoO or Co_3O_4–based electrodes reported in the literature.

Material	Preparation Method	Current Density [mAg^{-1}]	Cycle Number	Specific capacity [mAhg^{-1}]	Ref.
Co_3O_4/CNF	Chemical Deposition on Commercial CNFs	50	100	881	[29]
Co_3O_4/C nanowire	Electrospinning	100	20	534	[34]
CNF-Co_3O_4	Chemical Deposition on Commercial CNFs	100	50	>900	[35]
CoO/CNF	Electrospinning	140	100	854	[36]
CoO/Mesoporous carbon	Multi-step Chemical Processes	70	30	538	[30]
Co_3O_4/Graphene	Chemical Process	50	30	953	[6]
Co_3O_4/Graphene	Chemical Process	100	60	900	[37]
Co_3O_4/PCNF	**Electrospinning**	**100**	**100**	**952**	**Current study**

Conclusion

A facile, one-step electrospinning method was used to produce PCNFs incorporating uniformly-dispersed CoO_x nanoparticles that were encapsulated in onion-like graphene layers. The Co_3O_4 nanoparticles embedded in the porous structure of CNFs delivered excellent cyclic stability and high rate capability. The following can be highlighted from this study.

(i) The one-pot electrospinning method combined with a carefully designed heat treatment process allowed the formation of Co_3O_4 nanoparticles in a porous CNF matrix. Numerous pores were formed within the CNF matrix after the decomposition of PMMA precursor. These PCNFs not only can buffer the mechanical stresses arising from the lithiation/delithiation of the electrode but also can prevent the agglomeration of Co_3O_4 nanoparticles.

(ii) Co nanoparticles produced during the carbonization process served as a catalyst to graphitize the surrounded amorphous carbon. These onion-like graphene layers around the Co_3O_4 nanoparticles form a continuous conductive network within the conductive CNFs, contributing to reducing the ion/electron transfer resistance.

(iii) The onion-like graphene spheres served as sheaths to avoid the detachment of the nanoparticles from the CNF and helped maintain the integrity of the hybrid electrode material.

(iv) The Co_3O_4/PCNF electrode delivered a remarkable capacity of 952 mAg^{-1} after 100 cycles at a current density of 100 mAg^{-1}. The comparison of the electrochemical performance with similar CoO_x/C composites indicates that the above value is among the highest reported in the literature, suggesting this material is promising for high performance LIBs.

Acknowledgements

This project was financially supported by the Research Grants Council of Hong Kong SAR (GRF Project codes: 613811 and 613612). SA was the recipient of a Hong Kong PhD Fellowship Award. The authors also appreciate the technical assistance from the Materials Characterization and Preparation Facilities (MCPF) of HKUST.

Notes and references

[a] Department of Mechanical and Aerospace Engineering, The Hong Kong University of Science and Technology, Clear Water Bay, Hong Kong
*Email: mejkkim@ust.hk

Electronic Supplementary Information (ESI) available: [elemental mapping of the stabilized sample, general XPS spectra, TGA curve and cyclic performance of CNF and PCNF samples]. See DOI: 10.1039/b000000x/

1 V. Etacheri, R. Marom, R. Elazari, G. Salitra, D. Aurbach, *Energy Environ. Sci.* 2011, **4**, 3243
2 L. Ji, Z. Lin, M. Alcoutlabi, X. Zhang, *Energy Environ. Sci.* 2011, **4**, 2682
3 A. S. Arico, P. Bruce, B. Scrosati, J. M. Tarascon, W. V. Schalkwijk, *Nature Mater.* 2005, **4**, 366
4 B. Scrosati, *Electrochim. Acta* 2000, **45**, 2461
5 H. B. Wu, J. S. Chen, H. H. Hng, X. W. Lou, *Nanoscale* 2012, **4**, 2526
6 Z. S. Wu, W. Ren, L. Wen, L. Gao, J. Zhao, Z. Chen, G. Zhou, F. Li, H. M. Cheng, *ACS Nano* 2010, **4**, 3187
7 P. Poizot, S. Laruelle, S. Grugeon, L. Dupont, J. M. Tarascon, *Nature* 2000, **7**, 496
8 X. Wang, X. L. Wu, Y. G. Guo, Y. Zhong, X. Cao, Y. Ma, J. Yao, *Adv. Funct. Mater.* 2010, **20**, 1680
9 W. Y. Li, L. N. Xu, J. Chen, *Adv. Funct. Mater.* 2005, **15 (5)**, 851
10 M. V. Reddy, G. V. S. Rao, B. V. R. Chowdari, *Chem. Rev.* 2013, **113 (7)**, 5364
11 C. Zhang, X. Peng, Z. Guo, C. Cai, Z. Chen, D. Wexler, S. Li, H. Liu, *Carbon* 2012, **50**, 1897
12 B. Zhang, Y. Yu, Z.D. Huang, Y.B. He, D.H. Jang, W.S. Yoon, Y.W. Mai, F.Y. Kang, J.K. Kim, *Energy Environ. Sci*. 2012, **5**, 9895
13 L. Li, G. Zhou, X. Y. Shan, S. Pei, F. Li, H. M. Cheng, *J. Power Sources* 2014, **255**, 52
14 X. He, Y. Wu, F. Zhao, J. Wang, K. Jiang, S. Fan, *J. Mater. Chem. A*, 2013, **1**, 11121
15 S. A. Needham, G. X. Wang, K. Konstantinov, V. Tournayre, Z. Lao, H. K. Liu, *Electrochem. Solid St.* 2006, **9 (7)**, A315
16 V. Thavasi, G. Singh, S. Ramakrishna, *Energy Environ. Sci.* 2008, **1**, 205
17 S. Agarwal, A. Greiner, J. H. Wendorff, *Prog. Polym. Sci.* 2013, **38**, 963
18 M. Inagaki, Y. Yang, F. Kang, *Adv. Mater.* 2012, **24**, 2547
19 B. Zhang, Z. L. Xu, Y. B. He, S. Abouali, M. Akbari Garakani, E. Kamali Heidari, F. Kang, J. K. Kim, *Nano Energy* 2014, **4**, 88
20 N. A. M. Barakat, B. Kim, S. J. Park, Y. Jo, M. H. Jung, H. Y. Kim, *J. Mater. Chem.* 2009, **19**, 7371
21 B. Zhang, Y. Yu, Z. L. Xu, S. Abouali, M. Akbari Garakani, Y. B. He, F. Kang, J. K. Kim, *Adv. Energy Mater.* 2013, DOI: 10.1002/aenm.201301448.
22 R. Dedryvere, S. Laruelle, S. Grugeon, P. Poizot, D. Gonbeau, J. M. Tarascon, *Chem. Mater.* 2004, **16**, 1056
23 M. C. Biesinger, B. P. Payne, A. P. Grosvenor, L. W. M. Lau, A. R. Gerson, R. S. C. Smart, *Appl. Surf. Sci.* 2011, **257**, 2717
24 S. C. Petitto, E. M. Marsh, G. A. Carson, M. Langell, *J Mol. Catal. A-Chem.* 2008, **281**, 49
25 H. P. Cong and S. H. Yu, *Cryst. Growth Des.* 2009, **9 (1)**, 210
26 B. Li, Y. Xie, C. Wu, Z. Li, J. Zhang, *Mater. Chem. Phys.* 2006, **99**, 479
27 U. Zielke, K. J. Huttinger, W. P. Hoffman, *Carbon* 1996, **34**, 983
28 H. J. Liu, S. H. Bo, W. J. Cui, F. Li, C. X. Wang, Y. Y. Xia, *Electrochim. Acta* 2008, **53**, 6497
29 W. Yao, J. Yang, J. Wang, L. Tao, Electrochim. Acta 2008, **53**, 7326
30 H. J. Liu, S. H. Bo, W. J. Cui, F. Li, C. X. Wang, Y. Y. Xia, Electrochim. Acta 2008, **53**, 6497
31 B. Zhang, Z. L. Xu, J. K. Kim, RSC Adv. 2014, **4**, 12298
32 Z. L. Xu, B. Zhang, Z.Q. Zhou, S. Abouali, M. Akbari Garakani, J. Huang, J. Q. Huang, J. K. Kim, *RSC Adv.* 2014, **4**, 22359
33 Y. Wang, H. J. Zhang, L. Lu, L. P. Stubbs, C. C. Wong, J. Lin, *ACS Nano* 2010, **4 (8)**, 4753
34 P. Zhang, Z. P. Guo, Y. Huang, D. Jia, H. K. Liu, *J. Power Sources* 2011, **196**, 6987
35 W. L. Yao, J. L. Wang, J. Yang, G. D. Du, *J. Power Sources* 2008, **176**, 369
36 W. H. Ryu, J. Shin, J. W. Jung, I. D. Kim, *J. Mater. Chem. A* 2013, **1**, 3239
37 D. Qiu, G. Bu, B. Zhao, Z. Lin, L. Pu, L. Pan, Y. Shi, *Mater. Lett.* 2014, **119**, 12

Graphical abstract